An Analysis of Peristaltic Flow of Finitely Extendable Nonlinear Elastic-Peterlin Fluid in Two-Dimensional Planar Channel and Axisymmetric Tube

Nasir Ali and Zaheer Asghar

Department of Mathematics and Statistics, International Islamic University, Islamabad 44000, Pakistan

Reprint requests to Z. A.; E-mail: zaheer_asghar@yahoo.com

Z. Naturforsch. **69a**, 462 – 472 (2014) / DOI: 10.5560/ZNA.2014-0028
Received December 11, 2013 / revised April 17, 2014 / published online June 18, 2014

We have investigated the peristaltic motion of a non-Newtonian fluid characterized by the finitely extendable nonlinear elastic-Peterlin (FENE-P) fluid model. A background for the development of the differential constitutive equation of this model has been provided. The flow analysis is carried out both for two-dimensional planar channel and axisymmetric tube. The governing equations have been simplified under the widely used assumptions of long wavelength and low Reynolds number in a frame of reference that moves with constant wave speed. An exact solution is obtained for the stream function and longitudinal pressure gradient with no slip condition. We have portrayed the effects of Deborah number and extensibility parameter on velocity profile, trapping phenomenon, and normal stress. It is observed that normal stress is an increasing function of Deborah number and extensibility parameter. As far as the velocity at the channel (tube) center is concerned, it decreases (increases) by increasing Deborah number (extensibility parameter). The non-Newtonian rheology also affect the size of trapped bolus in a sense that it decreases (increases) by increasing Deborah number (extensibility parameter). Further, it is observed through numerical integration that both Deborah number and extensibility parameter have opposite effects on pressure rise per wavelength and frictional forces at the wall. Moreover, it is shown that the results for the Newtonian model can be deduced as a special case of the FENE-P model.

Key words: Peristaltic Motion; FENE-P Fluid; Channel; Axisymmetric Tube.

1. Introduction

Newtonian fluids are easy to handle because they can be described by a single constitutive equation. However, due to the complex nature of non-Newtonian fluids it is not possible to describe them by a single constitutive equation. A number of non-Newtonian fluid models have been proposed and most of them have received special attention of researchers in different flow situations. Amongst these models Maxwell model, Jeffrey model, Oldroyd-B model, Burger's model, second-order model, third-order model etc. are widely used non-Newtonian models in the literature. But still there are some fluid models which are given less attention and one of those is the FENE-P fluid model. The FENE-P fluid model is nonlinear, and in this model, the stress and strain are related implicitly. The flow of viscoelastic fluids using FENE-P model is usually handled by simulation [1] or using some numerical technique [2]. It was Oliveira [3] who noticed that an analytic solution for such fluid model can be obtained in some situations like fully developed flow. The study of Oliveira [3] motivated us to look for an analytic solution of the problem of peristaltic transport using the FENE-P model.

The study of dynamics of non-Newtonian fluids is an active area of research. Some examples of non-Newtonian biofluids are blood, cervical mucus, chymes etc. The flow of such type of non-Newtonian biofluids occurs under a natural phenomenon called peristalsis. Peristalsis is one of the major mechanisms of biofluid transport in the human body. Particularly, peristalsis occurs in transporting the bile in the bile duct, mixing of food, movement of chyme in the small intestines, and in the vasomotion of small blood vessels. Peristalsis has also been exploited for the industrial and mechanical purposes, as a result of which we see the roller and finger pumps that are designed to

transport the fluid without making contact to the internal moving parts, and in this way the contamination by the industrial wastage could be avoided. Moreover, a heart-lung machine is another device which operates on the principle of peristalsis.

Since the influential work of Latham [4], a number of theoretical and experimental investigations have been reported in literature. It is also worth mentioning that the mathematical modeling of the problems related to peristaltic transport started with the works of Shapiro et al. [5], who made the analysis in the wave frame of reference, and Fung and Yih [6], who performed the analysis in the laboratory frame. Shapiro's [5] approach has been adopted in larger part of the reported literature on peristaltic transport of Newtonian and non-Newtonian fluids. Particularly, this approach could be seen in the works [7 – 35].

Most of the works on peristaltic motion have been done using a Newtonian fluid model, see e. g. [7 – 15]. Such contributions are also of great values but their applications are limited only for the flow analysis in ureter. Since most of the biological and industrial fluids are non-Newtonian, therefore one will have to choose some non-Newtonian fluid model for the flow analysis relevant to biology and industry. From literature review one comes to know that peristaltic transport of non-Newtonian fluids have been receiving attention for the last few years which could be seen from the works [16 – 35], where different non-Newtonian fluid models namely, Maxwell fluid, Herschel–Bulkley fluid, order fluid, Jeffrey fluid, Walter's B fluid, and grade fluids have been used. However, limited numbers of studies are available in the literature regarding peristaltic flows under the widely used assumptions of long wavelength and low Reynolds number which use differential models like Oldroyd-B, oldroyd-4 constant. Giesekus, FENE-P etc. The FENE-P constitutive equation is based on the kinetic theory of polymers and has been extensively used for correlating exponential data for shear and extensional viscosities, transient and normal stress differences of polymer solutions. Further, it can predict decreasing viscosity with shear and is capable of modeling viscometric properties for a large class of fluids like polymeric liquids etc.

Paper pulps are the polymer solutions and chyme that is a biological fluid is defined as pulpy acidic fluid. The FENE-P model is a very common rheological constitutive equation for polymeric liquids; therefore due to analogy of chyme with pulps, it can be used to describe rheological properties of chyme in studying peristaltic transport of chyme. The dynamics of nutrients like amino acids which are also polymeric liquids, can be studied by using this model. The FENE-P model can also be used to study the motion of spermatozoa in the mucus filled female reproductive tract. During their journey to the ovum, sperm cells are both actively swimming and passively transported by peristaltic-like flows. Moreover, this model may also help in bioengineering for measuring viscometric properties of biofluids.

Keeping the importance of non-Newtonian fluids in mind, the present work is an attempt to analyze peristaltic flow of such fluids using a viscoelastic fluid model known as FENE-P model. The flow analysis is performed both in a two-dimensional channel and an axisymmetric tube. An analytical solution has been obtained in both cases. As stated earlier, most of the time simulation is required for the flow analysis of the FENE-P model due to its nonlinear nature. Therefore, the analytical solution such as obtained in this work is very useful because it can be incorporated as inlet boundary condition in simulations of more complex peristaltic flow of a FENE-P fluid. Under the highlighted aspects for the usefulness of the FENE-P model, the present analysis will hopefully prove to be a valuable contribution in the literature.

2. Formulation of the Problem

The dumbbell model with the Warner force law and Peterlin approximation for the average spring force is called FENE-P model. This model was rooted in kinetic theory and was initially developed to represent the behavior of dilute polymer solutions. The kinetic theory assumes that the motion of the dumbbells is the combined result of the hydrodynamic force, the Brownian motion force, and the connector force. This model leads to a differential constitutive equation that was provided in the form of an extra stress tensor in Bird et al. [36]. Following Chilcott and Rallison [37], we prefer to work with the model given in the form of configuration tensor $\mathbf{A}$, defined by $\mathbf{A} = 3\langle \mathbf{RR} \rangle / R_e^2$, in which $\mathbf{R}$ is an end-to-end vector that connects the dumbbell beads, $\langle \cdot \rangle$ represents an ensemble average over the configuration space, and R_e is the characteristic length. The connector force of the spring in the original FENE model follows the expression in [38], proposed by Warner

$$\mathbf{F}^{(c)} = \frac{H_0}{1-(\mathbf{R}\cdot\mathbf{R})/R_0^2}\mathbf{R}, \tag{1}$$

where H_0 is the Gaussian stiffness in the limit of small molecular extension, and R_0 is the maximum allowable dumbbell length. The nonlinearity in (1) induces the non-closure problem usually encountered in many areas of statistical physics, and a closed form constitutive equation is not possible unless an approximation is made. A well-known approximation was made by Peterlin [39]. According to which the configuration dependent nonlinear factor in (1) is replaced by a self-consistently averaged term. Thus we can write

$$\mathbf{F}^{(c)} \approx \frac{H_0}{1-\langle\mathbf{R}^2\rangle/R_0^2}\mathbf{R} \equiv fH_0\mathbf{R}, \tag{2}$$

where $\langle R^2\rangle$ is already defined and $(\equiv)$ means the identically equivalent. After making use of the configuration tensor, we note that the dimensionless function f gets the form [38],

$$f = f(\mathrm{tr}\mathbf{A}) = \frac{L^2}{L^2-\mathrm{tr}\mathbf{A}}. \tag{3}$$

Here L^2 is a measure of the extensibility of the dumbbells and is defined as $L^2 = 3R_0^2/R_e^2$. It is also related to b $(= H_0R_0^2/kT)$ by $L^2 = b+3$ as was used in [36], where k is the Boltzmann constant and T the absolute temperature.

Now the ensemble averaging of equations of motion for dumbbells yield the following evolution equation for $\mathbf{A}$ ([36], [40]):

$$\overset{\nabla}{\mathbf{A}} = -\frac{1}{\lambda_1}(f\mathbf{A}-a\mathbf{I}). \tag{4}$$

Equation (4) must be used in conjunction with the Kramer's relation for polymeric stress,

$$\bar{\tau} = \frac{\eta_p}{\lambda_1}(f\mathbf{A}-a\mathbf{I}). \tag{5}$$

In above equations, η_p is the zero shear rate polymer viscosity, λ_1 the relaxation time, and a is a parameter that depends on the extensibility parameter L^2 by $a = 1/(1-3/L^2)$. The parameter a has the relation with the physical properties by $a = 1+(3kT/H_0R_0^2)$ and is also related to b by $a = 1+(3/b)$. Moreover, the symbol $^\nabla$ represents Oldroyd's upper convected derivative which is defined by

$$\overset{\nabla}{\mathbf{A}} = \frac{\mathrm{D}\mathbf{A}}{\mathrm{D}t} - \mathbf{A}\nabla\bar{\mathbf{V}} - (\nabla\bar{\mathbf{V}})^*\mathbf{A}, \tag{6}$$

in which $\mathrm{D}/\mathrm{D}t$ is the material derivative defined by $\mathrm{D}/\mathrm{D}t = \partial/\partial t + \bar{\mathbf{V}}\cdot\nabla$. $\bar{\mathbf{V}}$ is the velocity vector and * denotes the transpose. On combining (4) and (5), we get

$$\overset{\nabla}{\mathbf{A}} = -\bar{\tau}/\eta_p. \tag{7}$$

Generally, the operator $\mathrm{D}/\mathrm{D}t$ satisfies the equation

$$\frac{\mathrm{D}}{\mathrm{D}t}(f\mathbf{A}) = f\left(\overset{\nabla}{\mathbf{A}}\right) + \mathbf{A}\frac{\mathrm{D}f}{\mathrm{D}t} \tag{8}$$

for any function f. For the two-dimensional unsteady flow in a planar channel, the material derivative is of the form

$$\frac{\mathrm{D}}{\mathrm{D}t} = \frac{\partial}{\partial\bar{t}} + \bar{U}\frac{\partial}{\partial\bar{X}} + \bar{V}\frac{\partial}{\partial\bar{Y}}, \tag{9}$$

where $\bar{U}$ and $\bar{V}$ are the velocity components in $\bar{X}$ and $\bar{Y}$, respectively. Whereas for axisymmetric case the material derivative is

$$\frac{\mathrm{D}}{\mathrm{D}t} = \frac{\partial}{\partial\bar{t}} + \bar{V}_{\bar{R}}\frac{\partial}{\partial\bar{R}} + \bar{V}_{\bar{Z}}\frac{\partial}{\partial\bar{Z}} \tag{10}$$

in which $\bar{V}_{\bar{R}}$ and $\bar{V}_{\bar{Z}}$ are also the velocity components in radial and axial directions, respectively.

If we apply the upper convected operator $^\nabla$ to (5), we find

$$\overset{\nabla}{\bar{\tau}} = \frac{\eta_p}{\lambda_1}\left(\left(f\overset{\nabla}{\mathbf{A}}\right) - a\overset{\nabla}{\mathbf{I}}\right) = \frac{\eta_p}{\lambda_1}\left(\left(f\overset{\nabla}{\mathbf{A}}\right) + 2a\mathbf{D}\right). \tag{11}$$

Here we used the result $\overset{\nabla}{\mathbf{I}} = -2\mathbf{D}$, with the rate of strain tensor denoted by

$$\mathbf{D} = \frac{1}{2}\left(\nabla\bar{V} + (\nabla\bar{V})^*\right). \tag{12}$$

2.1. Flow in a Planar Channel

Consider the peristaltic transport of an incompressible fluid in a two-dimensional channel of width $2a_1$. The flow is caused by the sinusoidal wave trains propagating on the channel walls with constant speed c. The shape of the wall surface is described by the same expression as in [19],

$$H(\bar{X},\bar{t}) = a_1 + b_1\left[\cos\left(\frac{2\pi}{\lambda}\left(\bar{X}-c\bar{t}\right)\right)\right], \tag{13}$$

in which b_1 is the amplitude of the wave, λ the wavelength, c the wave speed, $\bar{t}$ the time, $(\bar{X},\bar{Y})$ are the rectangular coordinates with $\bar{X}$-axis directed along the channel and $\bar{Y}$-axis transverse to it. The geometry of the problem is given in Figure 1.

The Cauchy stress tensor ($\bar{\mathbf{T}}$) is of the form

$$\bar{\mathbf{T}} = -\bar{P}\bar{\mathbf{I}} + \bar{\tau}\,. \tag{14}$$

Here $\bar{P}$ is the pressure, $\bar{\mathbf{I}}$ the identity tensor, and $\bar{\tau}$ is the extra stress tensor. The basic equations governing the flow in laboratory frame $(\bar{X},\bar{Y})$ are

$$\frac{\partial \bar{U}}{\partial \bar{X}} + \frac{\partial \bar{V}}{\partial \bar{Y}} = 0\,, \tag{15}$$

$$\rho\left(\frac{\partial}{\partial \bar{t}} + \bar{U}\frac{\partial}{\partial \bar{X}} + \bar{V}\frac{\partial}{\partial \bar{Y}}\right)\bar{U} = -\frac{\partial \bar{P}}{\partial \bar{X}} + \frac{\partial}{\partial \bar{X}}\bar{\tau}_{\bar{X}\bar{X}} + \frac{\partial}{\partial \bar{Y}}\bar{\tau}_{\bar{X}\bar{Y}}\,, \tag{16}$$

$$\rho\left(\frac{\partial}{\partial \bar{t}} + \bar{U}\frac{\partial}{\partial \bar{X}} + \bar{V}\frac{\partial}{\partial \bar{Y}}\right)\bar{V} = -\frac{\partial \bar{P}}{\partial \bar{Y}} + \frac{\partial}{\partial \bar{X}}\bar{\tau}_{\bar{Y}\bar{X}} + \frac{\partial}{\partial \bar{Y}}\bar{\tau}_{\bar{Y}\bar{Y}}\,, \tag{17}$$

where ρ is the fluid density, $\bar{U}$ and $\bar{V}$ are horizontal and vertical components of velocity.

The usual steady analysis can be performed by switching from laboratory frame $(\bar{X},\bar{Y})$ to the wave frame $(\bar{x},\bar{y})$. The following relationships between coordinates, velocities, and pressures in the two frames hold:

$$\bar{x} = \bar{X} - c\bar{t}\,,\ \ \bar{y} = \bar{Y}\,,\ \ \bar{u} = \bar{U} - c\,,\ \ \bar{v} = \bar{V}\,,\quad \bar{p}(\bar{x},\bar{y}) = \bar{P}\big(\bar{X},\bar{Y},\bar{t}\big)\,, \tag{18}$$

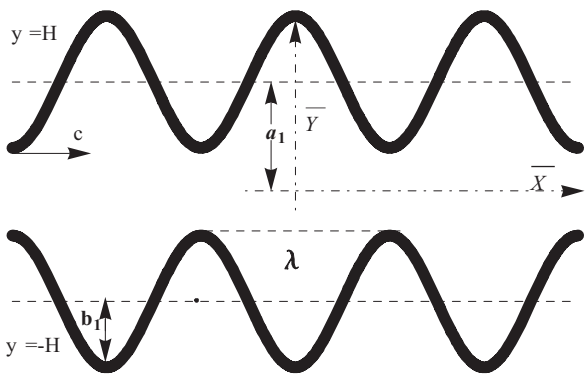

Fig. 1. Geometry of the problem.

where $\bar{u}$, $\bar{v}$, and $\bar{p}$ are the velocity components and pressure in the wave frame, respectively. For two-dimensional flows it is convenient to define the stream function (ψ) as

$$u = \frac{\partial \psi}{\partial y}\,,\ \ v = -\frac{\partial \psi}{\partial x}\,. \tag{19}$$

Upon making use of (18), (19) and defining the dimensionless quantities as

$$x = \frac{\bar{x}}{\lambda}\,,\ \ y = \frac{\bar{y}}{a_1}\,,\ \ u = \frac{\bar{u}}{c}\,,\ \ v = \frac{\bar{v}}{c\delta}\,,\ \ t = \frac{\pi c\bar{t}}{\delta}\,,\quad p = \frac{\delta a_1 \bar{p}}{\eta_{\mathrm{p}} c}\,,\ \ h = \frac{\bar{h}}{a_1}\,,\ \ \tau = \frac{a_1}{c\eta_{\mathrm{p}}}\bar{\tau}\,, \tag{20}$$

we find that (15) is identically satisfied whereas (9), (13), (16), and (17) take the form

$$\frac{\mathrm{D}}{\mathrm{D}t} = \delta\left(\frac{\partial \psi}{\partial y}\frac{\partial}{\partial x} - \frac{\partial \psi}{\partial x}\frac{\partial}{\partial y}\right), \tag{21}$$

$$h(x) = 1 + \phi\cos 2\pi x\,, \tag{22}$$

$$\mathrm{Re}\delta\left(\psi_y\frac{\partial}{\partial x} - \psi_x\frac{\partial}{\partial y}\right)\psi_y = -\frac{\partial p}{\partial x} + \delta\frac{\partial}{\partial x}\tau_{xx} + \frac{\partial}{\partial y}\tau_{xy}\,, \tag{23}$$

$$-\mathrm{Re}\delta^3\left(\psi_y\frac{\partial}{\partial x} - \psi_x\frac{\partial}{\partial y}\right)\psi_x = -\frac{\partial p}{\partial y} + \delta^2\frac{\partial}{\partial x}\tau_{yx} + \delta\frac{\partial}{\partial y}\tau_{yy}\,. \tag{24}$$

The wave number δ, Reynolds number Re, and amplitude ratio ϕ are defined through the following relations:

$$\delta = \frac{a_1}{\lambda}\,,\ \ \mathrm{Re} = \frac{\rho c a_1}{\eta_{\mathrm{p}}}\,,\ \ \phi = \frac{b_1}{a_1}(<1)\,. \tag{25}$$

In view of long wavelength approximation [25, 26], (21) gives $\mathrm{D}/\mathrm{D}t = 0$. Using this result in (8) and then incorporating the resulting equation in (11), we obtain an equation that yields an explicit relation between $\overset{\nabla}{\bar{\tau}}$ and $\overset{\nabla}{\mathbf{A}}$ that is

$$\overset{\nabla}{\bar{\tau}} = \frac{\eta_{\mathrm{p}}}{\lambda_1}\left(f\overset{\nabla}{\mathbf{A}} + 2a\mathbf{D}\right). \tag{26}$$

On equating (26) with (7), we obtain the final form for the FENE-P model in terms of extra stress tensor:

$$f\bar{\tau} + \lambda_1\overset{\nabla}{\bar{\tau}} = 2a\eta_{\mathrm{p}}\mathbf{D}\,. \tag{27}$$

Now it is desired to express f in terms of $\bar{\tau}$, for which first we took the trace of (5) and get

$$\mathrm{tr}\mathbf{A} = \frac{3a + \frac{\lambda_1}{\eta_p}\mathrm{tr}\bar{\tau}}{f}. \tag{28}$$

Using above equation in (3), we find

$$f = 1 + \frac{3a + (\lambda_1/\eta_p)(\mathrm{tr}a(\bar{\tau}))}{L^2}. \tag{29}$$

Upon making use of (12) and the definition of the upper convected derivative from (6), the component form of (27) in fixed frame $(\bar{X}, \bar{Y})$ can be written as

$$f\bar{\tau}_{\bar{X}\bar{X}} + \lambda_1\left\{\left(\frac{\partial}{\partial\bar{t}} + \bar{U}\frac{\partial}{\partial\bar{X}} + \bar{V}\frac{\partial}{\partial\bar{Y}}\right)\bar{\tau}_{\bar{X}\bar{X}} - \left((\nabla\bar{V})^*\bar{\tau}\right)_{\bar{X}\bar{X}} - \left(\bar{\tau}(\nabla\bar{V})\right)_{\bar{X}\bar{X}}\right\} = a\eta_p\left(\nabla\bar{V} + (\nabla\bar{V})^*\right)_{\bar{X}\bar{X}}, \tag{30}$$

$$f\bar{\tau}_{\bar{X}\bar{Y}} + \lambda_1\left\{\left(\frac{\partial}{\partial\bar{t}} + \bar{U}\frac{\partial}{\partial\bar{X}} + \bar{V}\frac{\partial}{\partial\bar{Y}}\right)\bar{\tau}_{\bar{X}\bar{Y}} - \left((\nabla\bar{V})^*\bar{\tau}\right)_{\bar{X}\bar{Y}} - \left(\bar{\tau}(\nabla\bar{V})\right)_{\bar{X}\bar{Y}}\right\} = a\eta_p\left(\nabla\bar{V} + (\nabla\bar{V})^*\right)_{\bar{X}\bar{Y}}, \tag{31}$$

$$f\bar{\tau}_{\bar{Y}\bar{Y}} + \lambda_1\left\{\left(\frac{\partial}{\partial\bar{t}} + \bar{U}\frac{\partial}{\partial\bar{X}} + \bar{V}\frac{\partial}{\partial\bar{Y}}\right)\bar{\tau}_{\bar{Y}\bar{Y}} - \left((\nabla\bar{V})^*\bar{\tau}\right)_{\bar{Y}\bar{Y}} - \left(\bar{\tau}(\nabla\bar{V})\right)_{\bar{Y}\bar{Y}}\right\} = a\eta_p\left(\nabla\bar{V} + (\nabla\bar{V})^*\right)_{\bar{Y}\bar{Y}}. \tag{32}$$

After using (18)–(20) in (29)–(31) and then employing the long wavelength and low Reynolds number assumptions on the resulting equations (23) and (24), we have

$$0 = -\frac{\partial p}{\partial x} + \frac{\partial}{\partial y}\tau_{xy}, \quad 0 = -\frac{\partial p}{\partial y}, \tag{33}$$

$$f\tau_{xx} = 0, \quad f\tau_{xy} = \mathrm{De}\tau_{xx}\psi_{yy} + a\psi_{yy}, \quad f\tau_{yy} = 2\mathrm{De}\tau_{xy}\psi_{yy}. \tag{34}$$

From (33) and (34) we arrive at

$$f = 1 + \frac{3a + \left(\frac{2\mathrm{De}^2}{a}\right)\left(\tau_{xy}\right)^2}{L^2}, \quad \tau_{xy} = \left(y\frac{\partial p}{\partial x} + A_1\right), \quad \tau_{yy} = \frac{2\mathrm{De}\left(\tau_{xy}\right)^2}{a} = \mathrm{tr}a(\tau), \quad \tau_{xx} = 0, \tag{35}$$

where A_1 is a constant of integration. The boundary conditions in the wave frame are the same as in [13]

$$\psi = 0, \quad \frac{\partial u}{\partial y} = \frac{\partial^2\psi}{\partial y^2} = 0 \ \text{ at } \ y = 0, \tag{36}$$

$$\psi = q, \quad \frac{\partial\psi}{\partial y} = -1 \ \text{ at } \ y = h, \tag{37}$$

$$\theta - 1 = q = \int_0^h \mathrm{d}y = \psi(h) - \psi(0), \tag{38}$$

where θ and q are the dimensionless mean flow rates in the fixed and wave frames, respectively.

By means of (35) and the second boundary condition in (36), we obtain the following expression of velocity gradient from (34):

$$\frac{\partial^2\psi}{\partial y^2} = \frac{p_x y}{a}\left(1 + \frac{3a + (2\mathrm{De}^2/a)p_x^2y^2}{L^2}\right). \tag{39}$$

Since $(1 + \frac{3a}{L^2})/a$ is unity by definition of a, we can write (39) as

$$\frac{\partial^2\psi}{\partial y^2} = \frac{\partial u}{\partial y} = p_x y\left(1 + \frac{2\mathrm{De}^2}{a^2L^2}p_x^2y^2\right). \tag{40}$$

Integrating (46) and making use of the first condition in (36) and the second condition in (37), we get the following expression of the stream function:

$$\psi = -y - \frac{\mathrm{d}p}{\mathrm{d}x}\left(\left(\frac{1}{2}\right)(h^2y - y^3/3) + \left(\frac{5\beta}{4}\right)\left(h^4y - \frac{y^5}{5}\right)\left(\frac{\mathrm{d}p}{\mathrm{d}x}\right)^2\right). \tag{41}$$

Now using the remaining boundary condition in (37), i. e., $\psi = q$ at $y = h$, we find

$$\frac{\mathrm{d}p}{\mathrm{d}x} = \left[-2(2^{1/3})h^8\beta + 2^{2/3}\left(-27\beta^2(h+q)h^{10} + \sqrt{\beta^3h^{20}(4h^4 + 729(h+q)^2\beta)}\right)^{2/3}\right]\left[6h^5\beta\left(-27\beta^2 \cdot (h+q)h^{10} + \sqrt{\beta^3h^{20}\left(4h^4 + 729(h+q)^2\beta\right)}\right)^{1/3}\right]^{-1}, \tag{42}$$

where $\beta = 2\mathrm{De}^2/5a^2L^2$. The pressure rise per wavelength ΔP_λ and frictional forces F_λ on the wall are defined as

$$\Delta P_\lambda = \int_0^1 \left(\frac{\mathrm{d}p}{\mathrm{d}x}\right)\mathrm{d}x, \tag{43}$$

$$F_\lambda = \int_0^1 h^2\left(-\frac{\mathrm{d}p}{\mathrm{d}x}\right)\mathrm{d}x. \tag{44}$$

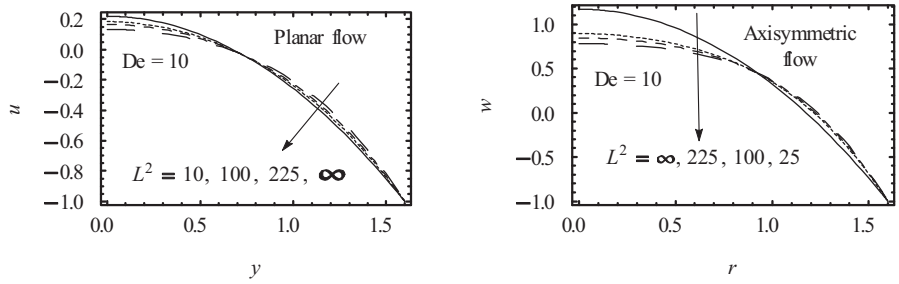

Fig. 2. Velocity profile for different values of extensibility parameter L^2 with $\theta = 0.7$, $\phi = 0.6$.

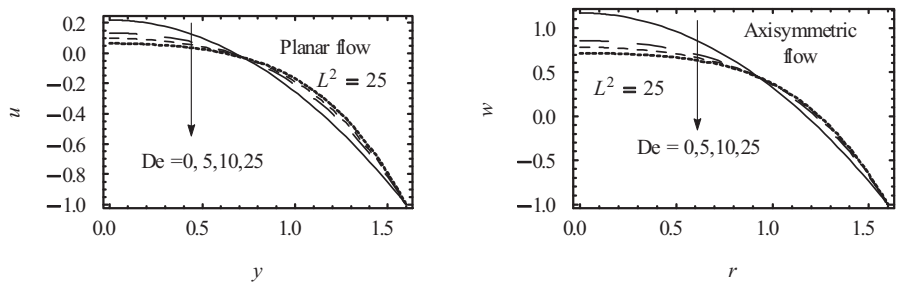

Fig. 3. Velocity profile for different values of Deborah number De with $\theta = 0.7$, $\phi = 0.6$.

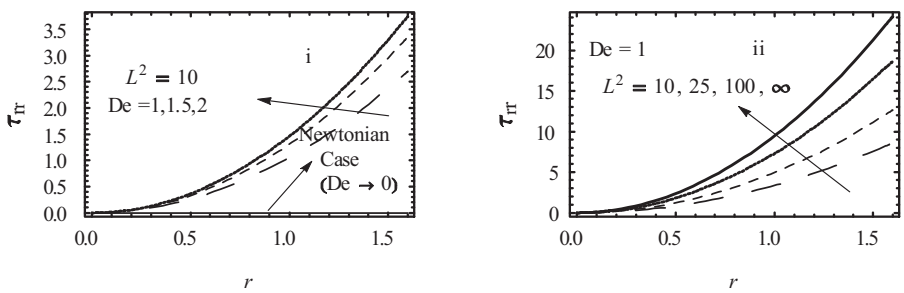

Fig. 4. Normal Stress profile in the axisymmetric case with $\theta = 0.7$, $\phi = 0.6$.

2.2. Flow in an Axisymmetric Tube

Before proceeding we mention here that the alternative notations for coordinates, velocity components, and stresses will be used for the flow in an axisymmetric tube, and the rest of the quantities/parameters will be denoted by the same symbols as used in the previous section. Now we consider the peristaltic transport of an incompressible viscoelastic fluid represented by the FENE-P model in a flexible axisymmetric tube of radius a_1. In cylindrical coordinates $(\bar{R},\bar{Z})$ the shape of tube wall is given as

$$\bar{H}(\bar{Z},\bar{t}) = a_1 + b_1\left[\cos\left(\frac{2\pi}{\lambda}(\bar{Z}-c\bar{t})\right)\right]. \tag{45}$$

The flow is governed by the following equations:

$$\frac{1}{\bar{R}}\frac{\partial}{\partial\bar{R}}\left(\bar{R}\bar{V}_{\bar{R}}\right) + \frac{\partial\bar{V}_{\bar{Z}}}{\partial\bar{Z}} = 0, \tag{46}$$

$$\rho\left(\frac{\partial}{\partial\bar{t}} + \bar{V}_{\bar{R}}\frac{\partial}{\partial\bar{R}} + \bar{V}_{\bar{Z}}\frac{\partial}{\partial\bar{Z}}\right)\bar{V}_{\bar{R}} = -\frac{\partial\bar{P}}{\partial\bar{R}} + \frac{1}{\bar{R}}\frac{\partial}{\partial\bar{R}}\left(\bar{R}\bar{\tau}_{\bar{R}\bar{R}}\right) + \frac{\partial}{\partial\bar{Z}}\bar{\tau}_{\bar{R}\bar{Z}}, \tag{47}$$

$$\rho\left(\frac{\partial}{\partial\bar{t}} + \bar{V}_{\bar{R}}\frac{\partial}{\partial\bar{R}} + \bar{V}_{\bar{Z}}\frac{\partial}{\partial\bar{Z}}\right)\bar{V}_{\bar{Z}} = -\frac{\partial\bar{P}}{\partial\bar{Z}} + \frac{1}{\bar{R}}\frac{\partial}{\partial\bar{R}}\left(\bar{R}\bar{\tau}_{\bar{Z}\bar{R}}\right) + \frac{\partial}{\partial\bar{Z}}\bar{\tau}_{\bar{Z}\bar{Z}}, \tag{48}$$

where $\bar{V}_{\bar{R}}$ and $\bar{V}_{\bar{Z}}$ are radial and axial components of velocity, respectively.

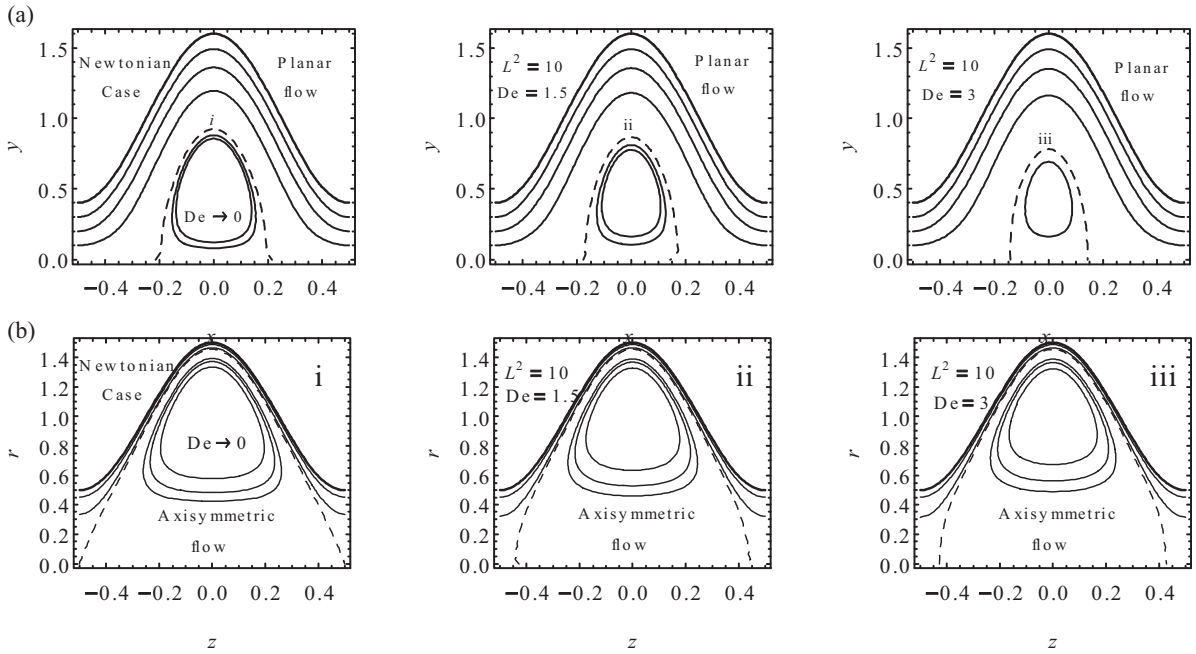

Fig. 5. (a) Streamlines for the variation of Deborah number De with $\theta = 0.6$, $\phi = 0.6$. (b) Streamlines for the variation of Deborah number De with $\theta = 0.5$, $\phi = 0.5$.

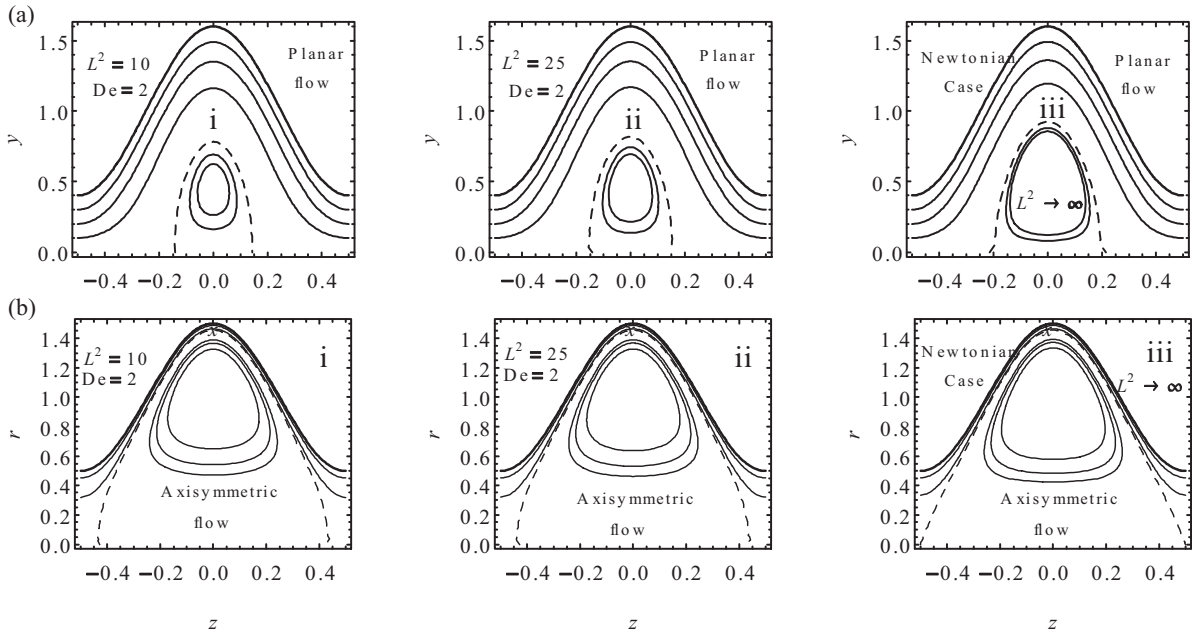

Fig. 6. (a) Streamlines for the variation of extensibility parameter L^2 with $\theta = 0.6$, $\phi = 0.6$. (b) Streamlines for the variation of extensibility parameter L^2 with $\theta = 0.5$, $\phi = 0.5$.

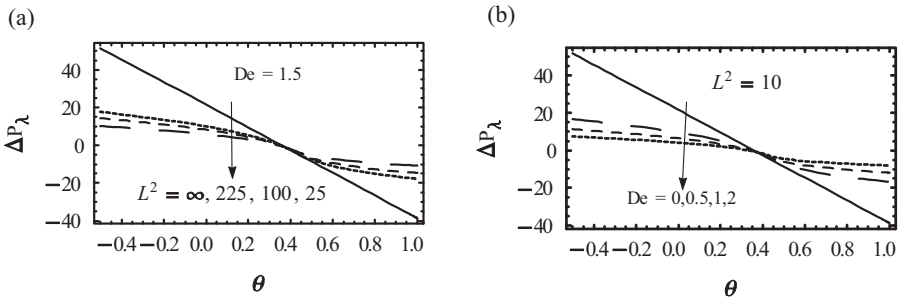

Fig. 7. Pressure rise per wavelength ΔP_λ with $\phi = 0.5$.

The coordinates, velocities, and pressures in the laboratory frame $(\bar{R},\bar{Z})$ and the wave frame $(\bar{r},\bar{z})$ are related through the following expressions:

$$\begin{aligned} &\bar{z} = \bar{Z} - c\bar{t}\,,\ \ \bar{r} = \bar{R}\,,\ \ \bar{v}_{\bar{z}} = \bar{V}_{\bar{Z}} - c\,, \\ &\bar{v}_{\bar{r}} = \bar{V}_{\bar{R}}\,,\ \ \bar{p}(\bar{r},\bar{z}) = \bar{P}\big(\bar{R},\bar{Z},\bar{t}\big)\,, \end{aligned} \tag{49}$$

where $\bar{v}_{\bar{z}}$, $\bar{v}_{\bar{r}}$ are the axial and radial components of velocity, respectively, and $\bar{p}$ is the pressure in the wave frame. Making use of (49), defining the dimensionless variables as

$$\begin{aligned} &z = \frac{\bar{z}}{\lambda}\,,\ \ r = \frac{\bar{r}}{a_1}\,,\ \ v_z = \frac{\bar{v}_{\bar{z}}}{c}\,,\ \ v_r = \frac{\bar{v}_{\bar{r}}}{c\delta}\,, \\ &t = \frac{\pi c\bar{t}}{\delta}\,,\ \ p = \frac{\delta a_1 \bar{p}}{\eta_{\mathrm{p}} c}\,,\ \ h = \frac{\bar{h}}{a_1}\,,\ \ \tau = \frac{a_1}{c\eta_{\mathrm{p}}}\bar{\tau} \end{aligned}$$

and the stream function by

$$v_r = -\frac{1}{r}\frac{\partial\psi}{\partial z}\,,\ \ v_z = \frac{1}{r}\frac{\partial\psi}{\partial r}\,, \tag{50}$$

(46) is identically satisfied and in addition by applying the long wavelength and low Reynolds number assumptions (47), (48), and the component form of the equations for extra stress tensor like in the planar case reduce to

$$0 = -\frac{\partial p}{\partial r}\,,\ \ 0 = -\frac{\partial p}{\partial z} + \frac{1}{r}\frac{\partial(r\tau_{zr})}{\partial r}\,, \tag{51}$$

$$\begin{aligned} &f\tau_{rr} = 2\mathrm{De}\tau_{zr}\frac{\partial}{\partial r}\left(\frac{1}{r}\frac{\partial\psi}{\partial r}\right), \\ &f\tau_{rz} = \mathrm{De}\tau_{zz}\frac{\partial}{\partial r}\left(\frac{1}{r}\frac{\partial\psi}{\partial r}\right) + a\frac{\partial}{\partial r}\left(\frac{1}{r}\frac{\partial\psi}{\partial r}\right), \\ &f\tau_{zz} = 0\,. \end{aligned} \tag{52}$$

After little manipulation, we can have

$$\begin{aligned} &\tau_{rz} = \left(\frac{\partial p}{\partial z}\right)\frac{r}{2} + \frac{A_2}{r}\,,\ \ f = 1 + \frac{3a + (2\mathrm{De}^2/a)(\tau_{rz})^2}{L^2}\,, \\ &\tau_{rr} = \frac{2\mathrm{De}(\tau_{rz})^2}{a} = \mathrm{tr}a(\tau)\,,\ \ \tau_{zz} = 0\,, \end{aligned} \tag{53}$$

where A_2 is the constant of integration. The boundary conditions in the wave frame are defined as [20]

$$\psi = 0\,,\ \ \frac{\partial}{\partial r}\left(\frac{1}{r}\frac{\partial\psi}{\partial r}\right) = 0 \ \text{ at } \ r = 0\,, \tag{54}$$

$$\psi = q\,,\ \ \frac{1}{r}\frac{\partial\psi}{\partial r} = -1 \ \text{ at } \ r = h\,, \tag{55}$$

$$\begin{aligned} \theta - \frac{1}{2}\left(1 + \frac{\phi^2}{2}\right) = q &= \int_0^h \frac{\partial\psi}{\partial r}\,\mathrm{d}y \\ &= \psi(h) - \psi(0)\,. \end{aligned} \tag{56}$$

Now adopting the same procedure as described in Section 2.1, we arrive at the following expressions for stream function and axial pressure gradient:

$$\begin{aligned} \psi = &-\frac{r^2}{2} + \frac{1}{2}\frac{\mathrm{d}p}{\mathrm{d}z}\left(\frac{1}{8}\big(2h^2r^2 - r^4\big)\right. \\ &\left. + \frac{\beta}{2}\big(3h^4r^2 - r^6\big)\left(\frac{\mathrm{d}p}{\mathrm{d}z}\right)^2\right), \end{aligned} \tag{57}$$

$$\begin{aligned} \frac{\mathrm{d}p}{\mathrm{d}z} = &\Bigg[-6^{2/3}h^{10}\beta + 6^{1/3}\Bigg(-144\beta^2(h^2+2q)h^{12} \\ &+ \sqrt{6}\sqrt{\beta^3h^{24}\big(h^6 + 3456\big(h^2+2q\big)^2\beta\big)}\Bigg)^{2/3}\Bigg]\Bigg[12h^6\beta \\ &\cdot\Bigg(-144\beta^2(h^2+2q)h^{12} \\ &+ \sqrt{6}\sqrt{\beta^3h^{24}\big(h^6 + 3456\big(h^2+2q\big)^2\beta\big)}\Bigg)^{1/3}\Bigg]^{-1}, \end{aligned} \tag{58}$$

where $\beta = \mathrm{De}^2/24a^2L^2$. The pressure rise per wavelength ΔP_λ and frictional forces F_λ can be obtained

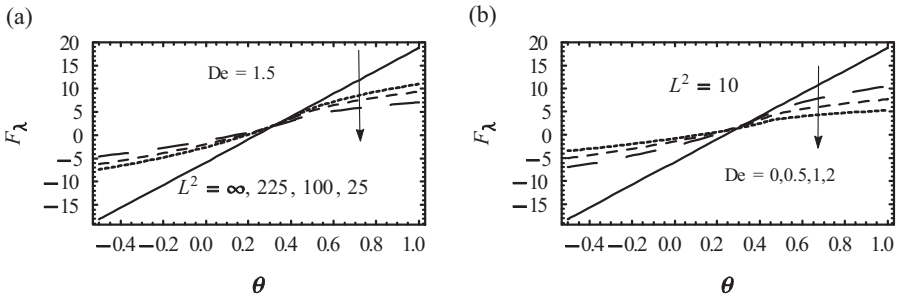

Fig. 8. Frictional forces F_λ with $\phi = 0.5$.

through the following formulas:

$$\Delta P_\lambda = \int_0^1 \left(\frac{\mathrm{d}p}{\mathrm{d}z}\right) \mathrm{d}z, \tag{59}$$

$$F_\lambda = \int_0^1 h^2 \left(-\frac{\mathrm{d}p}{\mathrm{d}z}\right) \mathrm{d}z. \tag{60}$$

3. Discussion of the Results

We break up this section into three subsections namely, flow behavior, trapping and pumping phenomena. The detail of these subsections is as follows:

3.1. Flow Behavior

This part describes the effects of De and L^2 on the velocity profile and the normal stresses which are depicted in Figures 2–4. Here we observe that these parameters leave the opposite effects on the velocity profile but the same effects on the normal stresses. From Figures 2 and 3 we observe that the magnitude of the velocity increases at the centre of the channel with the increase of L^2 but decreases by increasing De. We also note that the magnitude of the velocity profile is greater for axisymmetric flow compared with the case of planar flow. Here it is important to note that the results for a Newtonian fluid can be obtained when either De $\to 0$ or $L^2 \to \infty$. A departure from Newtonian behavior is observed for small values of L^2 or large values of De. In fact the velocity profile shows shear thinning behavior and become flatter as $L^2 \to \infty$ or De $\to 0$. We also observe that the velocity field is parabolic for both the Newtonian and the FENE-P fluids. Figure 4 highlights the effects of De and L^2 on normal stresses for the axisymmetric case. It is seen that the normal stresses increase by increasing these parameters.

3.2. Trapping Phenomenon

This subsection describes the effects of pertinent parameters on trapping phenomenon through Figures 5 and 6. Figure 5a,b shows the effects of De on trapping for fixed value of L^2. We observe that the size of the trapped bolus decreases by increasing De. Moreover, the size of the trapped bolus is greater in the case of axisymmetric flow when compared with the planar flow. From Figure 6a,b, we observe that L^2 leaves the opposite effects on trapping phenomenon in comparison with De. Thus we may interpret from all these figures that size and circulation of the trapped bolus reduces for a shear-thinning fluid in comparison with Newtonian fluid.

3.3. Pumping Phenomenon

Here our focus is to explore the effects of FENE-P model parameters on pressure rise per wavelength ΔP_λ and frictional forces F_λ. For the analysis we have performed numerical integration for the evaluation of integrals appearing in (43), (44), (59), and (60) using Mathematica. The results are shown in Figures 7 and 8. We have depicted the results only for the axisymmetric case, and one can easily observe the same effects for the channel flow only with qualitative differences, i. e., pressure rise attains higher values in the axisymmetric case compared with the planar case.

Figure 7 shows the effects of De and L^2 on ΔP_λ. Since the peristaltic flow shows different interesting behaviors, Figure 7 is divided into following four subregions:

- The region in which $\Delta P_\lambda > 0$ and $\theta < 0$ is called retrograde pumping region.
- The region where $\Delta P_\lambda > 0$ and $\theta > 0$ is called peristaltic pumping region.

- Third region corresponds to $\Delta P_\lambda = 0$, which is called free pumping region.
- The region in which $\Delta P_\lambda < 0$ but $\theta > 0$ is called augmented pumping region.

Figure 7 shows that ΔP_λ decreases by increasing the flow rate θ. Moreover, ΔP_λ shows a linear behavior for the Newtonian case whereas nonlinear behavior for the FENE-P fluid. We also note that De and L^2 leave the opposite effect on ΔP_λ in the retrograde and peristaltic pumping regions, i. e. ΔP_λ decreases (increases) by increasing De (L^2). However, in the augmented pumping region the situation is reversed. As already mentioned, large values of De or small values of L^2 correspond to a shear thinning fluid. Then we may conclude from Figure 7a and b that ΔP_λ in the peristaltic pumping region is greater for a Newtonian fluid in comparison with the shear thinning fluid. Such observations are also reported in some previous studies [28, 29].

Figure 8 presents the variation of frictional force F_λ against the mean flow rate θ for different values of De and L^2. From this figure we see that F_λ increases by increasing θ and show linear behavior for the Newtonian case whereas nonlinear behavior for the FENE-P fluid. We observe from Figure 8a that F_λ resists the flow till $\theta \approx 0.3$ and gets weak after this critical value. The resistance provided by F_λ is greater for the Newtonian fluid in comparison with the shear thinning fluid. The effect of De on the frictional forces is opposite to that of L^2 and also with a different value of flow rate $\theta = 0.27$.

4. Concluding Remarks

From the presented analysis we conclude that Deborah number De and extensibility parameter L^2 leave opposite effects on flow characteristics, trapping and pumping phenomena. Specifically, we find that the velocity field attains higher values at the centre of the channel for the case of axisymmetric flow when compared with the planar flow. Moreover, the velocity profile decreases (increases) by increasing De (L^2) at the centre of the channel whereas it shows an opposite trend near the walls. The velocity field is parabolic both for Newtonian and FENE-P fluids. As for normal stress is concerned, it increases by increasing both De and L^2. If we look into the pumping phenomenon we come to know that ΔP_λ increases in the retrograde, peristaltic, and free pumping regions, whereas it decreases in the augmented pumping region by increasing L^2. The effects of De on ΔP_λ are quite opposite to that of L^2. In addition, F_λ resist the flow below a certain critical value of the flow rate and this resistance increases in going from FENE-P to Newtonian fluid. Furthermore, F_λ shows a linear behavior for the Newtonian case whereas its behavior is nonlinear for the FENE-P fluid. Coming on the trapping phenomenon, we infer that the size of trapped bolus reduces by increasing De while it increases by increasing L^2.

Acknowledgements

We are very thankful to the referees for their valuable and constructive suggestions which lead to significant improvement of the work.

[1] R. B. Bird, P. J. Dotson, and N. L. Jhonson, J. Non-Newton. Fluid Mech. **11**, 69 (1982).
[2] D. O. Olagunju, App. Math. Comp. **173**, 213 (1980).
[3] P. J. Oliveira, App. Math. Comp. **158**, 157 (2002).
[4] T. W. Latham, Fluid Motion in a Peristaltic Pump, M. S. Thesis, MIT, Cambridge 1966.
[5] A. H. Shapiro, M. Y. Jaffrin, and S. L. Weinberg, J. Fluid Mech. **37**, 799 (1969).
[6] Y. C. Fung and C. S. Yih, ASME J. Appl. Mech. **35**, 669 (1968).
[7] S. Takabatake and K. Ayukawa, J. Fluid Mech. **122**, 439 (1982).
[8] O. Eytan, A. J. Jaffa, J. H. Toov, E. Dalach, and D. Elad, Ann. Biomed. Eng. **27**, 372 (1999).
[9] M. Mishra and A. R. Rao, Z. Angew. Math. Phys. **53**, 532 (2003).
[10] E. F. Elshehawey, N. T. Eldabe, E. M. Elghazy, and A. Ebaid, Appl. Math. Comp. **182**, 140 (2006).
[11] Kh. S. Mekheimer and Y. Abd Elmaboud, Phys. Lett. A. **372**, 1657 (2008).
[12] A. Ebaid, Phys. Lett. A **372**, 4493 (2008).
[13] S. Nadeem and N. S. Akbar, Commun. Nonlin. Sci. Numer. Simul. **14**, 3844 (2009).
[14] T. Hayat and Z. Asghar, Z. Naturforsch. **65a**, 697 (2010).
[15] S. Srinivas, R. Gayathri, and M. Kothandapani, Comp. Phys. Commun. **180**, 2115 (2009).
[16] A. M. Siddiqui and W. H. Schwarz, J. Non-Newton. Fluid Mech. **53**, 257 (1994).
[17] Kh. S. Mekheimer, Biorheology. **39**, 755 (2002).
[18] K. Vajravelu, S. Sreenadh, and V. R. Babu, Appl. Math. Comput. **169**, 726 (2005).

[19] M. Elshahed and M. H. Haroun, Math. Prob. Eng. **6**, 663 (2005).
[20] T. Hayat and N. Ali, Appl. Math. Comput. **188**, 1491 (2007).
[21] T. Hayat, N. Ali, and S. Asghar, Phys. Lett. A. **363**, 397 (2007).
[22] T. Hayat, M. Javed, and N. Ali, Transp. Porous Med. **74**, 259 (2008).
[23] S. Nadeem and N. S. Akbar, J. Taiwan Inst. Chem. Eng. **42**, 67 (2011).
[24] O. U. Mehmood, S. Shafie, and N. Mustapha, Int. J. Appl. Math. Mech. **7**, 1 (2011).
[25] N. S. Akbar and S. Nadeem, Int. J. Heat Mass Trans. **55**, 3964 (2012).
[26] O. U. Mehmood, N. Mustapha, and S. Shafie, Appl. Math. Mech. Engl. **33**, 1313 (2012).
[27] M. Mustafa, S. Hina, T. Hayat, and A. Alsaedi, Int. J. Heat Mass Trans. **55**, 4871 (2012).
[28] N. Ali, Y. Wang, T. Hayat, and M. Oberlack, Biorheology. **45**, 611 (2008).
[29] N. Ali, Y. Wang, T. Hayat, and M. Oberlack, Can. J. Phys. **87**, 1047 (2009).
[30] Kh. S. Mekheimer. S. R. Komy, and S. I. Abdelsalam, Chin. Phys. B **22**, 124702 (2013).
[31] Kh. S. Mekheimer and M. A. El Kot, Appl. Math. Model. **36**, 5393 (2012).
[32] Y. Abdelmaboud, Kh. S. Mekheimer, and A. I. Abdellateef, J. Heat Trans. **135**, 44502 (2013).
[33] N. S. Akbar, S. Nadeem, R. Ul Haq, and Z. H. Khan, J. Comput. Theor. Nanosci. **11**, 47 (2014).
[34] S. Akram, Kh. S. Mekheimer, and S. Nadeem, Appl. Math. Inf. Sci. **8**, 1127 (2014).
[35] N. S. Akbar and S. Nadeem, Meccanica **49**, 325 (2014).
[36] R. B. Bird, P. J. Dotson, and N. L. Johnson, J. Non-Newton. Fluid Mech. **7**, 213 (1980).
[37] M. D. Chilcott and J. M. Rallison, J. Non-Newton. Fluid Mech. **29**, 381 (1988).
[38] R. R. Huilgol and N. Phan-Thien, Fluid Mechanics of Viscoelasticity, Elsevier, Amsterdam, Lausanne, New York, Oxford, Shannon, Tokyo 1997.
[39] A. Peterlin, J. Polym. Sci., Polym. Lett. B **4**, 287 (1966).
[40] B. Purnode and M. J. Crochet, J. Non-Newton. Fluid Mech. **77**, 1 (1998).